Biophysical Journal
Article

Biophysical Society

Dynamics of asymmetric membranes and interleaflet coupling as intermediates in membrane fusion

Marcos Arribas Perez[1] and Paul A. Beales[1,2,*]
[1]Astbury Centre for Structural Molecular Biology and School of Chemistry, University of Leeds, Leeds LS2 9JT, UK and [2]Bragg Centre for Materials Research, University of Leeds, Leeds LS2 9JT, UK

ABSTRACT Membrane fusion is a tool to increase the complexity of model membrane systems. Here, we use silica nanoparticles to fuse liquid-disordered DOPC giant unilamellar vesicles (GUVs) and liquid-ordered DPPC:cholesterol (7:3) GUVs. After fusion, GUVs display large membrane domains as confirmed by fluorescence confocal microscopy. Laurdan spectral imaging of the membrane phases in the fused GUVs shows differences compared with the initial vesicles indicating some lipid redistribution between phase domains as dictated by the tie lines of the phase diagram. Remarkably, using real-time confocal microscopy we were able to record the dynamics of formation of asymmetric membrane domains in hemifused GUVs and detected interleaflet coupling phenomena by which the DOPC-rich liquid-disordered domains in outer monolayer modulates the phase state of the DPPC:cholesterol inner membrane leaflet which transitions from liquid-ordered to liquid-disordered phase. We find that internal membrane stresses generated by membrane asymmetry enhance the efficiency of full fusion compared with our previous studies on symmetric vesicle fusion. Furthermore, under these conditions, the liquid-disordered monolayer dictates the bilayer phase state of asymmetric membrane domains in >90% of observed cases. By comparison to the findings of previous literature, we suggest that the monolayer phase that dominates the bilayer properties could be a mechanoresponsive signaling mechanism sensitive to the local membrane environment.

SIGNIFICANCE Biomembranes present asymmetric lipid composition between their two leaflets. This asymmetry has a strong impact on the properties and behaviors of the membrane. However, producing asymmetric model membranes is nontrivial, making the study of related biophysical mechanisms challenging. Here, we present an experimental framework to image the dynamics of asymmetric membrane domains formed as transient intermediates during the fusion of GUVs. We observe interleaflet coupling in asymmetric membranes, where liquid-disordered domains dominate. By comparison with previous literature, this may indicate that the phase state of asymmetric membranes can be mechanoresponsive to its local environment. Furthermore, enhanced full fusion efficiency of these GUVs indicates that stresses generated by membrane asymmetry can promote the formation of the full fusion pore.

INTRODUCTION

Biological membranes are formed by a myriad of different lipids that provide them with particular biophysical properties and functionality (1). The organization of lipids within the membrane can lead to lateral heterogeneities where liquid-ordered (L_o) and liquid-disordered (L_d) phases separate into coexisting membrane domains (1–3). In cell membranes, lipid domains are transient and nanoscopic (<200 nm) and, hence, difficult to characterize experimentally (3–6). For this reason, biomimetic model membranes, such as giant unilamellar vesicles (GUVs) and giant plasma membrane vesicles, which can display larger and more stable microdomains, have been extensively employed to study the lateral organization of lipids within phase-separated membranes (1).

In addition to lateral heterogeneities, biological membranes also exhibit differences in the lipid content of each leaflet. This membrane asymmetry is conserved across organisms of all living kingdoms and plays a fundamental role in numerous cellular functions (7,8). Early studies proved the asymmetric distribution of just phospholipid

Submitted August 4, 2022, and accepted for publication October 4, 2022.

*Correspondence: p.a.beales@leeds.ac.uk

Editor: Ilya Levental.

https://doi.org/10.1016/j.bpj.2022.10.006

headgroups (9,10), but Lorent et al. recently demonstrated that the plasma membrane of human erythrocytes is also asymmetric in the degree of saturation of the acyl chains, with the inner leaflets enriched in lipids with polyunsaturated acyl chains (11). Membrane asymmetry has represented a problem to understand the formation of L_o domains in the plasma membrane, since they exist in both leaflets but only the outer monolayer presents the appropriate lipid composition to form such structures (12,13). The reason behind the formation of bilayer domains is that the two monolayers are coupled, so one can modulate the physical state of the other and thus determine the physicochemical properties of the membrane bilayer (4,6,13). Nevertheless, the mechanisms governing the interleaflet coupling phenomena are still not clear and might involve many different physicochemical parameters, such as line tension, surface tension at the bilayer midplane, acyl chain interdigitation, membrane fluctuations, curvature, and differential lateral stress (4,6,7).

Commonly, studies on lipid lateral organization use GUVs prepared from solutions containing a mixture of the desired lipids to display phase separation. Similarly, most investigations of membrane asymmetry rely on model membranes directly produced with different lipid compositions in each leaflet. However, alternative methods to induce phase separation in initially homogeneous membranes can provide a more precise control over the final membrane composition and a better understanding on the dynamic processes behind the lipid organization within the membrane. Membrane fusion represents a potential strategy to fulfill this purpose. Bezlyepkina et al. used electrofusion to generate three component GUVs from simpler vesicles and determine the tie lines of ternary lipid mixtures in the final GUV (14). In addition, membrane phase separation can also be of great importance in synthetic biology as a spatiotemporal regulation system of membrane-protein interactions and membrane remodeling processes. For instance, Dreher et al. showed that phase separation can lead to the division of a L_d - L_o GUV into two single-phased daughter vesicles, one formed by the disordered phase and the other by the ordered phase (15). They then used DNA-triggered membrane fusion to induce phase separation in the daughter GUVs and repeat the division process (15). Other studies have also employed fusion-based strategies to generate asymmetric GUVs (16,17).

Previously, we showed that silica nanoparticles (SiO_2 NPs) of 30 nm diameter effectively mediate fusion of DOPC GUVs by imposing a balance between membrane curvature and increased lateral tension in the membranes (18). Local enhancement of membrane curvature and tension mimics the physical mechanisms of native SNARE proteins. This increase in membrane tension and high local membrane curvature, plus lipid packing defects induced by the SiO_2 NPs, would lead to the exposure of hydrophobic membrane regions to the environment. Therefore, the membranes can reorganize so that the exposed region of one membrane matches the exposed hydrophobic region of the neighboring membrane forming a hemifusion stalk, which is the first intermediate stage of a fusion process. From this point, we have proposed that if the membrane tension is high enough, the energy barriers associated with the opening of a fusion pore is rapidly overcome and the vesicles directly fuse. Otherwise, the fusion occurs via less-energy-demanding processes involving hemifusion intermediate states. Here, we use the same type of SiO_2 NPs to mediate membrane fusion between L_d and L_o GUVs with the aim to generate phase-separated GUVs. The fusions between L_d and L_o GUVs show mechanistic differences compared with fusions between two DOPC GUVs, indicating that differences in the properties of each fusing membrane might help to promote the opening of the final fusion pore. Moreover, by recording the fusion process we visualize changes in lipid lateral organization, asymmetric domain formation, and interleaflet coupling phenomena experienced by hemifused GUVs.

MATERIALS AND METHODS

Materials

Lipids 1,2-dioleoyl-*sn*-glycero-3-phosphocholine (DOPC), 1,2-dipalmitoyl-*sn*-glycero-3-phosphocholine (DPPC), cholesterol (Chol) from ovine wool, and 1,2-dioleoyl-*sn*-glycero-3-phosphoethanolamine-*N*-(lissamine rhodamine B sulfonyl) (ammonium salt) (Rh-DOPE) were purchased from Avanti Polar Lipids (Alabaster, AL). 3,3′-dioctadecyloxacarbocyanine perchlorate (DiO), and 6-dodecanoyl-2-dimethylaminonaphthalene (Laurdan) were purchased from Thermo Fisher Scientific (Loughborough, UK). Naphtho[2,3-*a*]pyrene (naphthopyrene) was obtained from Tokyo Chemical Industries UK (Oxford, UK). Silica nanoparticles LUDOX TM-50, HEPES, glucose, NaCl, and indium titanium oxide (ITO)-coated glass slides (surface resistivity 8–12 V sq^{-1}) were purchased from Sigma-Aldrich (Gillingham, UK). Microscope μ-slide 8-well glass-bottom chambers (Ibidi, Gräfelfing, Germany) were purchased from Thistle Scientific (Glasgow, UK).

Electroformation of GUVs

GUVs were prepared using the electroformation method (19). First, 15 μL of the desired lipid mixture in chloroform (0.7 mM) were deposited as a thin layer over the conductive side of two ITO-coated glass slides and then dried under a nitrogen stream. The lipid mixtures used were DOPC and 0.5 mol % Rh-DOPE for the L_d GUVs; and DPPC:Chol (7:3 mol ratio) with 1 mol % of naphthopyrene for the L_o GUVs. The ITO slides were then assembled into an electroformation chamber each in contact with a copper tape and separated by a 1.6 mm Teflon gasket. The chamber was filled with a 300 mM sucrose solution (300 mOsm/kg) and connected to a function generator to apply an AC electric field. The frequency of the electric field was set at 10 Hz and the voltage was gradually increased from 1 V peak-to-peak (Vpp) to 5 Vpp over 15 min and maintained at 5 Vpp for 2 h. Finally, the frequency was gradually reduced to 0.1 Hz over 10 min to facilitate the closure and detachment of GUVs from the slide. DOPC GUVs were prepared at room temperature, whereas DPPC:Chol (7:3) GUVs were prepared at 50°C above the melting temperature of DPPC (T_m of DPPC = 41°C). After electroformation, GUVs were suspended in isotonic buffer containing 20 mM HEPES and 150 mM NaCl (300 mOsm/kg) adjusted to pH 7.4.

The osmolality of the inner sucrose solution and the external buffer was measured with a 3320 Micro-Osmometer (Advanced Instruments, Norwood, UK).

Confocal imaging and analysis

Imaging was performed using a Zeiss LSM-880 inverted laser scanning confocal microscope with a Plan-Apochromat 40×/1.4 Oil DIC M27 objective lens (NA = 1.4). To detect the membrane phase DOPC GUVs were labeled with Rh-DOPE, which partitions into a L_d phase and DPPC:Chol (7:3) GUVs with naphthopyrene (Npy), which partitions into a L_o phase. A total of 100 μL of each population of GUVs were deposited into a well of a microscope slide previously passivated with a solution of 5% BSA for 10 min followed by rinsing with Milli-Q water. Once the GUVs were sunk to the bottom of the well, 25 μg/mL SiO_2 NPs were carefully added to the sample and we acquired time series to record fusion events in real time. Npy and Rh were excited with a 405 nm diode laser and a 561 nm diode pumped solid-state laser, respectively. The emission of Npy was recorded between 410 and 500 nm and the emission of Rh between 566 and 630 nm. Image analysis was performed with Fiji (ImageJ) and plotting and statistical analysis were carried out using Origin Pro. Real-time tile scanning was used to image large areas of the sample and the proportion of phase-separated GUVs in the sample after exposure to 25 μg/mL SiO_2 NPs was counted manually.

Laurdan spectral imaging

GUVs labeled with 0.5 mol % Laurdan were prepared by electroformation. The spectral images are acquired using the lambda mode of the Zeiss LSM880 confocal laser microscope, which allows splitting of the fluorescence emission spectrum of a dye into up to 34 spectral intervals recorded in individual detection channels. Laurdan was excited with the 405 nm laser and the fluorescence detection range was set between 410 and 550 nm with a spectral step of 8.9 nm per channel. Snapshots of Laurdan-labeled GUVs were acquired before and after exposure to NPs. The images were analyzed with a Fiji plugin developed by Sezgin et al. (20), setting 440 and 490 nm as maximum emission wavelengths to calculate the GP values using the following equation:

$$GP = \frac{I_{440} - I_{490}}{I_{440} + I_{490}},$$

where I_{440} and I_{490} are the fluorescence intensity at 440 and 490 nm, respectively.

RESULTS AND DISCUSSION

SiO_2 NPs mediate fusion between L_d and L_o GUVs

We first tested the ability of 30 nm SiO_2 NPs to promote fusion between a L_d GUV and a L_o GUV. Two populations of GUVs were prepared using electroformation, one made of DOPC (L_d GUVs) and the other composed of DPPC and Chol in a 7:3 mol ratio (L_o GUVs). The two populations of GUVs were mixed in a 1:1 volume ratio and incubated with 25 μg/mL of SiO_2 NPs. Experiments were performed at room temperature, below the melting temperature of DPPC ($T_m = 41°C$). To visualize the reorganization of the lipids in the membrane during the fusion process, we incorporated Rh-DOPE (0.5 mol %) to the L_d GUVs and Npy (1 mol %) into the L_o GUVs. These dyes are used as membrane phase markers as Rh-DOPE preferentially partitions into the L_d phase of the membrane and Npy into L_o domains (21). In our images we observe that on average the fluorescence intensity of Npy is around 7.5 times higher ($K_p = 7.5 \pm 1.4$) in L_o domains than in L_d domains, confirming the preferential partitioning of the dye into the L_o phase (Fig. S1 and Table S1).

Using real-time confocal microscopy, we observe that 30 nm SiO_2 NPs promotes fusion between a L_d GUV and a L_o GUV. Importantly, once fused, the membrane of the new GUV lowers its free energy by remaining phase separated, displaying large L_d and L_o microdomains (Fig. 1 and Video S1). Our observations are consistent with previous studies on membrane phase separation in DOPC:DPPC:Chol GUVs (22–24). From the size of the single-phase GUVs that are going to fuse, we can estimate the final lipid composition of the fused, phase-separated membrane. From the fusion events that we have observed, we obtained a range of lipid compositions from 67% DOPC:23% DPPC:10% cholesterol to 34% DOPC:46% DPPC:20% cholesterol. The average composition we get from all the analyzed images is 50.7% DOPC:34.5% DPPC:14.8% cholesterol (Table S2). These compositions fall on a straight line on the ternary phase diagram that joins the

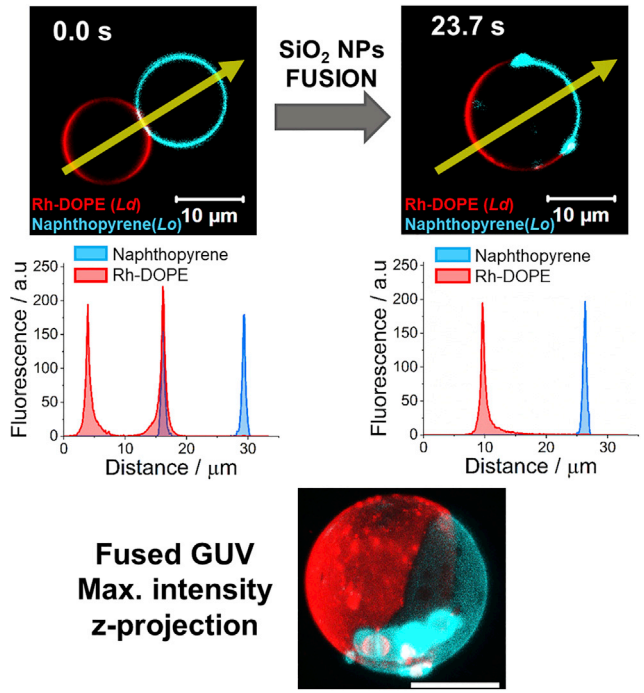

FIGURE 1 Confocal microscopy images of L_o and L_d GUVs before and after fusion. L_o DPPC/Chol (7:3) GUV is labeled with naphthopyrene (Npy) (*cyan*) and L_d DOPC GUV is labeled with Rh-DOPE (*red*). After fusion Npy partitions into the L_o phase and Rh-DOPE into the L_d phase. Plots show the fluorescence intensity profile of Rh-DOPE (*red*) and Npy (*blue*) along the yellow arrows shown in the micrographs. The bottom image shows a 3D maximum intensity projection of a phase-separated fused GUV. To see this figure in color, go online.

compositions of the two initial GUV that fuse. At room temperature, these ternary lipid compositions are in the liquid-liquid immiscibility region of the phase diagram, where L_d and L_o domains coexist in the membrane but close to the boundary where a third solid phase ($L_{\beta'}$) can appear (22–24) (Fig. S2). However, in the timescale of our experiments we do not see evidences of three coexisting phases in the membrane.

Further analysis of the membrane phase was performed using Laurdan spectral imaging. In this case, L_d GUVs and L_o GUVs were both labeled with 0.5 mol % Laurdan. In addition, 0.1 mol % Rh-DOPE was also added to the L_d GUVs. Control L_d GUVs show mean Laurdan GP values of -0.45 ± 0.02, while the GP values of L_o GUVs are much higher, peaking at 0.29 ± 0.03 (Fig. 2 *a*), as expected for more ordered membranes (20). After fusion, the Laurdan GP map clearly shows two easily distinguishable regions in the membrane, which correspond to the L_o (positive GP values) and L_d (negative GP values) domains (Fig. 2 *b*). Rh-DOPE fluorescence in the fused GUV matches perfectly with the region of the membrane displaying negative GP values, confirming their L_d nature (Fig. 2 *b*). Compared with the control DOPC GUVs, the L_d domains of the fused GUVs show significantly higher (less negative) average GP values ($GP = -0.10 \pm 0.05$), which indicates a denser lipid packing, while the GP values observed in the L_o domains of the fused GUVs are slightly less positive ($GP = 0.24 \pm 0.04$) than in the control DPPC:Chol GUVs (Fig. 2 *c*). After fusion, the lipids laterally redistribute between membrane domains until an equilibrium lipid composition, determined by the tie lines of the phase diagram, is reached. Consequently, the L_d phase of the fused GUV is no longer a pure DOPC membrane but a DOPC-rich domain, and the same occurs with the L_o phase, which is enriched in DPPC and cholesterol but not exclusively formed by these lipids.

From tile scan images, we quantified the average proportion of phase-separated GUVs generated after incubating the vesicles with the SiO_2 NPs to be $11 \pm 4\%$ (Fig. S3 *a*). This value does not show statistically significant difference with respect to the proportion of fused GUVs observed in samples of just DOPC GUVs in isosmotic conditions (18) (Fig. S3 *a*). These results demonstrate that the fusogenic activity of 30 nm SiO_2 NPs is not limited to DOPC membranes, but that they maintain their ability to promote fusion when one of the membranes is stiffer, as in the case of DPPC:Chol GUVs.

In a recent study, we observed that the fusion mediated by these SiO_2 NPs can follow three different pathways that we classified as direct full fusion, hemifusion-fusion, and gentle membrane merging, depending on the intermediate states that the GUVs adopt during the process (18). In the direct full fusion, the fusion occurred before any lipid transfer between the GUVs was detected, while the other two mechanisms involved lipid mixing indicative of hemifusion intermediate states. In the hemifusion-fusion processes, the hemifusion is followed by the opening of the fusion pore and full fusion of the vesicles. In contrast, in the gentle membrane-merging events, the fusion pore never opens following GUV hemifusion; instead, one GUV gradually shrinks while the other grows until there is only one final GUV with a volume equivalent to the sum to the initial vesicle volumes and a membrane formed by a mixture of the initial membranes. From our results we did not see any preferential pathway with 35% of the fusions following the direct full fusion pathway, 30% the hemifusion-fusion

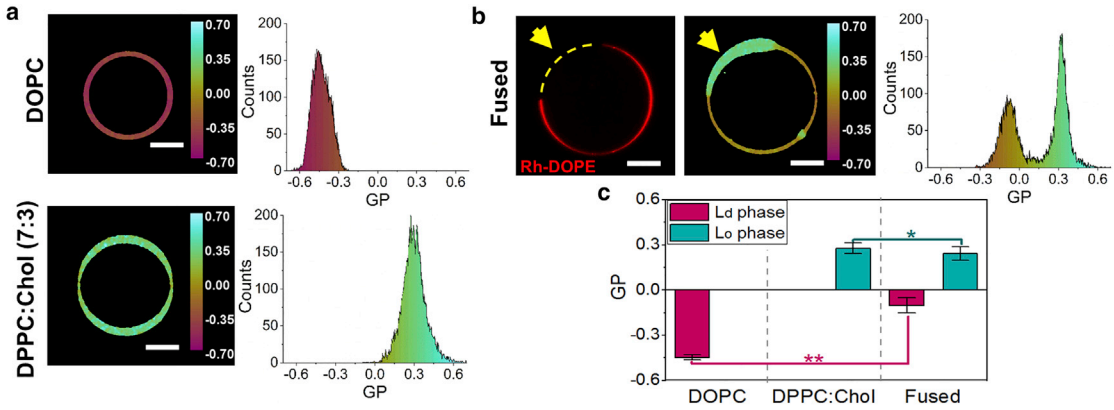

FIGURE 2 Laurdan GP of GUVs before and after fusion. (*a*) Example of Laurdan GP maps and histograms of DOPC GUV (*top*) and DPPC:Chol (7:3) GUV (*down*) GUVs. (*b*) Example of Rh-DOPE fluorescence (*left*), Laurdan GP map (*middle*), and GP histogram (*right*) of a fused GUV displaying phase separation. Rh-DOPE fluorescence matches with lower values of Laurdan GP (L_d phase) while it is excluded from the L_o domain, which shows positive GP values. (*c*) Bar plot of average GP values $\pm$SD of L_d and L_o phase in DOPC GUVs ($n = 26$), DPPC:Chol (7:3) GUVs ($n = 20$), and fused phase-separated GUVs ($n = 26$). The average GP value of the L_d phase is significantly less negative in the fused GUVs ($GP = -0.10 \pm 0.05$) than in the pure DOPC GUVs ($GP = -0.45 \pm 0.02$). The average GP of the L_o phase is slightly higher in the L_o GUVs ($GP = 0.29 \pm 0.03$) than in the fused phase-separated GUVs ($GP = 0.24 \pm 0.04$). The statistical significance was tested using a one-way ANOVA with Bonferroni multiple comparisons test ($^*p \leq 0.05$, $^{**}p \leq 0.01$). To see this figure in color, go online.

pathway and the remaining 35% undergoing gentle membrane merging (Fig. S3 *b*). We proposed that the fusion pathway followed by the GUVs would be primarily determined by the membrane tension, so fusing GUVs that do not have enough tension to overcome the energy cost associated to the opening and expansion of a fusion pore would follow the gentle membrane-merging pathway (18).

Here, we recorded 32 confocal microscopy time series of complete fusion events. The analysis of the movies showed that in just over half of the movies (53%, $n = 17$) the GUVs experienced a direct full fusion (Fig. 1, Video S1). In the other 15 observations (47%), we detected a hemifusion intermediate state before a fusion pore opens and the GUVs fuse. A more thorough analysis and discussion of the hemifusion processes will be provided later. Physically, the differentiation between the direct full fusion and the hemifusion-fusion pathways is one of kinetics. In the direct full fusion pathway, the full fusion pore opens on a rapid timescale where the hemifusion intermediate is not detectable with the temporal resolution of the time-resolved confocal imaging (frame rate = 3.33 Hz).

Interestingly, the gentle membrane-merging pathway, which represented 35% of the total fusions between two DOPC GUVs recorded in our previous study (18) (Fig. S3 *b*), is completely suppressed when one of the GUVs has a L_o membrane. The reason for the absence of gentle merging membrane events is unclear. One possibility is that the transbilayer asymmetry at the hemifusion diaphragm, formed by a DOPC monolayer and a DPPC:Chol monolayer, might make the membrane more unstable or increase the membrane tension and thus lower the energy barrier to the eventual opening of the fusion pore. Using flicker spectroscopy, Elani et al. demonstrated that asymmetric GUVs, with one leaflet composed of DOPC and the other with POPC, show a significantly increased membrane-bending rigidity compared with symmetric bilayers (25). Theoretical modeling and coarse-grained simulations have also suggested that imbalanced lipid packing in each leaflet of asymmetric membranes can generate a differential lateral stress that can have strong impact in the mechanical properties of the membrane, including membrane tension, bending rigidity, and spontaneous curvature (26). During the fusion of L_o and L_d GUVs, the increase of membrane tension that arises from the differential stress at the asymmetric hemifusion diaphragm would then provide the energy needed for the opening and expansion of a fusion pore. In asymmetric membranes where the tension between the two leaflets differ, the cholesterol would, in theory, flow from the less-tense into the more-tense monolayer to reduce the differential stress. In this case, the flow of cholesterol between leaflets could cancel the differential stress. However, the differential tension between each monolayer is not the only driver that determines the distribution of cholesterol. Cholesterol is known to have a preferential partition into regions of the membrane rich in saturated lipids (27), so this preferential partition into ordered phases would affect the amount of cholesterol located in each monolayer of the asymmetric membrane. This has been recently reported in a study by Varma and Deserno, where, using a combination of molecular dynamics simulations and theoretical models, they show that in asymmetry membranes the partition bias of cholesterol into ordered phases drives cholesterol to locate preferentially in the monolayer richer in saturated lipids (28). In that work, they conclude that the differential stress due to lipid packing asymmetry is not relieved by the flow of cholesterol between leaflets (28). Hence, we propose that, in our system, when the asymmetric hemifused membrane is formed, the cholesterol flow from the DPPC:Chol leaflet to the DOPC monolayer is limited and cannot relieve the differential stress at the hemifusion diaphragm. Our results therefore suggest an important role of the different lipid composition and phase state of each membrane in the opening of the full fusion pore in the last stage of the fusion process.

Notably, while the efficiency of opening of a full fusion pore is enhanced by asymmetric hemifused membrane intermediates, the kinetics of full fusion pore opening is not obviously changed. The relative proportion of fusion events that are categorized as direct full fusion and as hemifusion-fusion pathways remain comparatively equal, as also observed for the case of symmetric DOPC-DOPC GUV fusion (Fig. S3 *b*).

Hemifusion between L_d and L_o GUVs leads to membrane asymmetry and interleaflet coupling

In nearly half of the fusion events recorded ($n = 15$), the opening of the fusion pore was preceded by a hemifusion intermediate state. This initially gives rise to a metastable asymmetric membrane diaphragm during the fusion process. Figs. 3 *a* and S4 *a* show a confocal microscopy time lapse of two GUVs undergoing hemifusion along with fluorescence intensity data in different regions of their membranes. Maximum fluorescence intensity of rhodamine (Rh_{max}) corresponds to regions of the membrane where both leaflets are formed mainly by L_d DOPC lipids, whereas L_o bilayers show maximum fluorescence intensity of Npy (Npy_{max}). If the dyes were present in only one of the membrane monolayers, their fluorescence intensity would be ~50% lower than those maximum values.

When the GUVs become hemifused, Rh-DOPE fluorescence emerges in a region of the L_o membrane. The Npy fluorescence intensity in the same membrane region is simultaneously reduced to about half compared with its fluorescence in the rest of the membrane, Npy_{max} (Figs. 3 *a* and S4 *a*, Video S2). Assuming that only the outer leaflets of the GUVs are fused, the fluorescence intensities suggest that the L_o marker is only present in the inner membrane leaflet while the outer monolayer is enriched with DOPC lipids transferred from the opposite GUV, which induce a

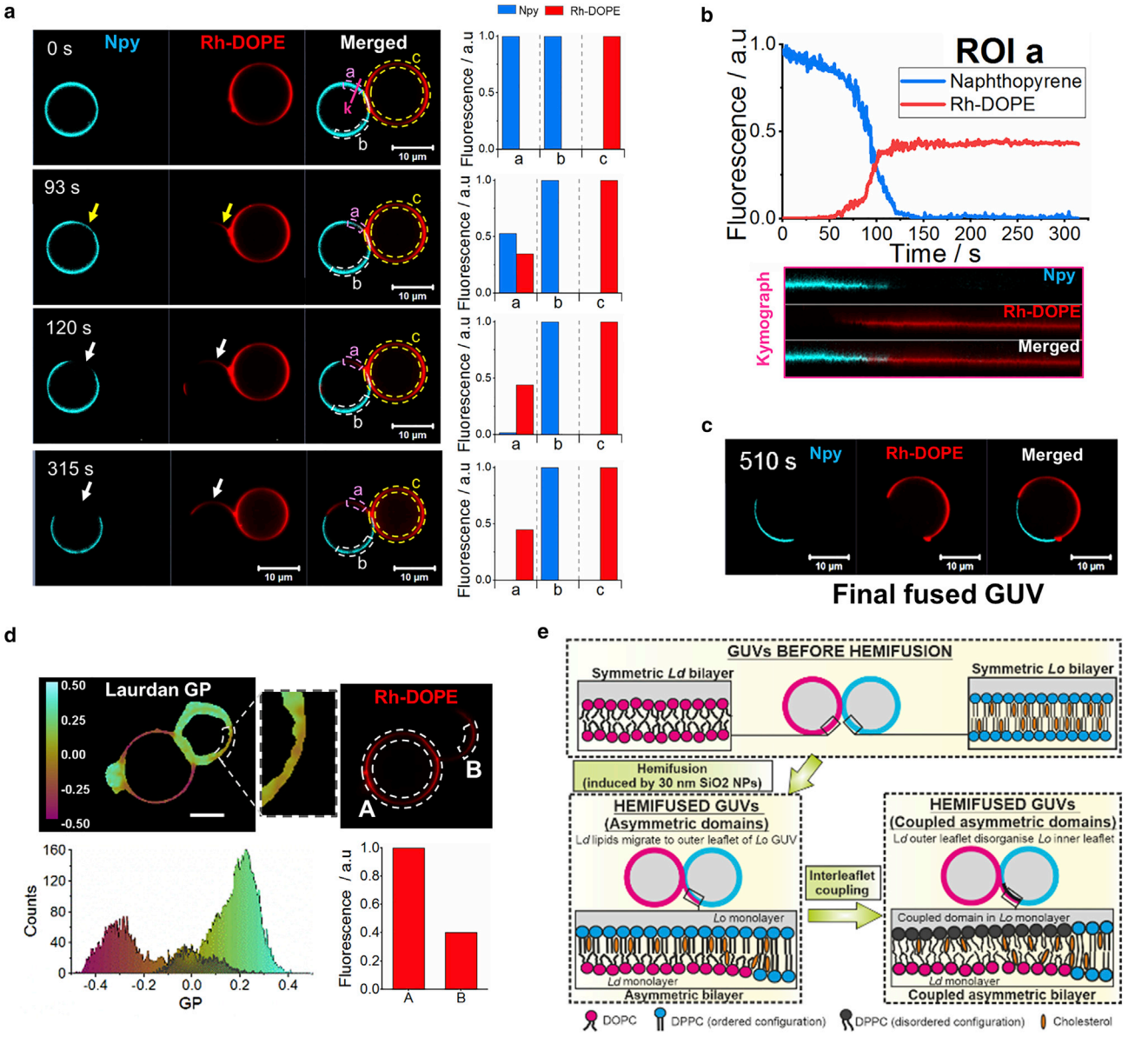

FIGURE 3 Asymmetric membrane domains and interleaflet coupling in hemifused GUVs. (*a*) Confocal microscopy time-lapse images of GUVs during hemifusion. Naphthopyrene (Npy) (*cyan*) and Rh-DOPE (*red*) are used as L_o and L_d markers, respectively. Yellow arrows indicate regions of the membrane where both dyes are colocalized (asymmetric domains) and white arrows indicate regions of the membrane where the Npy has been excluded from the membrane. Bar plots show the normalized fluorescence intensity measured in the ROIs a, b, and c shown in the merged channel. Fluorescence intensity in ROI b and ROI c corresponds to the maximum intensity of Npy and Rh-DOPE, respectively. ROI a shows an initial rise in Rh-DOPE intensity simultaneous to a reduction of Npy fluorescence to about half compared with its maximum (93 s micrograph). Later micrographs show a complete exclusion of Npy from that region of the membrane while the intensity of Rh-DOPE in ROI a remains close to 0.5. (*b*) Normalized fluorescence intensity of Rh-DOPE (*red line*) and Npy (*blue line*) in ROI a against time. Kymographs show the fluorescence intensity over time at the pink line indicated as "k" in the 0 s micrographs in (*a*). (*c*) Phase-separated GUV after full fusion. (*d*) Laurdan GP map (*left*) and localization of Rh-DOPE in the membrane (*right*) of a hemifused GUV. Zoomed region indicates a disordered domain within the initial L_o GUV that shows GP values (shaded in GP histogram) intermediate between the DOPC-rich membrane and the membrane enriched in DPPC and cholesterol. Fluorescence intensity of Rh-DOPE in ROI B denotes that the L_d marker is only present in one leaflet. (*e*) Schematic representation of asymmetric domain formation and interleaflet coupling during hemifusion between a L_d GUV and a L_o GUV. To see this figure in color, go online.

phase transition from L_o to L_d indicated by the rise of Rh-DOPE fluorescence. Hence, the structure in that region of the membrane would correspond to an asymmetric domain with an ordered DPPC:Chol inner leaflet and a disordered DOPC-rich outer monolayer (Fig. 3 *e*). In all the events observed, it is the Rh-DOPE fluorescence that is transferred to a region on the L_o vesicle and never the other way around.

Strikingly, shortly after the formation of the asymmetric domain, we observe a complete exclusion of the L_o marker from the domain while the fluorescence intensity of

Rh-DOPE remains close to 50% of Rh_{max} (Figs. 3 *a* and S4 *a*). The analysis of the fluorescence intensity dynamics in that membrane region clearly shows the transient colocalization of the two dyes followed by a rapid the loss of Npy fluorescence (Figs. 3 *b* and S4 *b*). The exclusion of Npy from the asymmetric domain likely corresponds to an interleaflet coupling phenomenon by which a disorganization in the DPPC:Chol inner monolayer is induced by the L_d outer leaflet, without noticeable interleaflet transfer of L_d-preferring lipids, to create symmetry in the phase structure of the bilayer despite the compositional asymmetry being retained. The resulting structure would be an asymmetric L_d domain where Rh-DOPE molecules partition into the DOPC-rich outer leaflet while the inner leaflet is composed of DPPC and cholesterol in a disorganized configuration, which compels the Npy molecules to diffuse laterally and partition to regions where the lipids are more densely packed in an L_o phase (Fig. 3 *e*). The loosening of the lipid packing within the asymmetric membrane domains was confirmed by Laurdan imaging (Fig. 3 *e*). The membrane asymmetry is only maintained while the GUVs are hemifused. Once the GUVs fully fuse, the membrane symmetry is restored and the location of the fluorescent dyes in one monolayer matches its location in the opposite monolayer (Figs. 3 *c* and S4 *c*).

Two of the videos that we categorized as hemifusion show dynamical changes in the membrane phase at an apparently extended hemifusion diaphragm. In those events, we observe the complete exclusion of the L_o marker from the membrane region where the GUVs come into contact (Fig. 4 and S5, Video S3). The exclusion of Npy occurs simultaneously to an expansion and flattening of the contact region and a decrease of the relative fluorescence intensity of Rh-DOPE. The relative fluorescence intensity of the latter dye is, however, slightly higher (∼70%) than 50%. This fluorescence intensity data make it difficult to confidently define the configuration adopted by the membrane. A possible scenario is that the observed structure is an expanded hemifusion diaphragm with a DOPC monolayer labeled with Rh-DOPE and a DPPC:Chol monolayer from which the Npy dye is excluded due to the interleaflet coupling. We speculate that the higher levels of Rh-DOPE fluorescence might be due to some extent of interleaflet lipid transfer, likely by a period of lipid flip-flop enhanced by membrane stresses during the initial hemifusion. The expanded hemifusion diaphragm dominated by the L_d phase shows a very short lifetime as it is formed just before the GUVs fully fuse. In these events, we do not detect migration of dyes from one GUV to the opposite. The dye-exclusion and phase dynamics associated with it are restricted to the presumed hemifusion diaphragm and the L_d - L_o phase boundaries locate at the edges of it, where the bilayer at the hemifusion diaphragm meets the bilayers of the L_d and L_o GUVs, forming a Y-like junction.

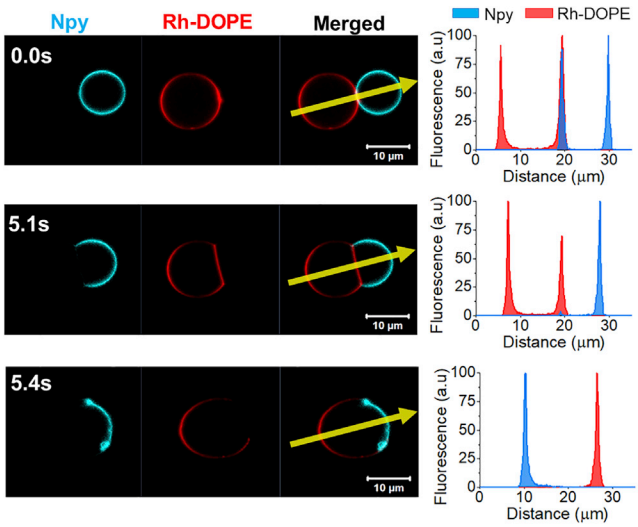

FIGURE 4 Confocal microscopy time-lapse micrographs showing naphthopyrene (Npy) exclusion from the GUV-GUV interface before full fusion. Naphthopyrene (Npy) (*cyan*) and Rh-DOPE (*red*) are used as L_o and L_d markers, respectively. Plots show the fluorescence intensity profile of Npy (*blue*) and Rh-DOPE (red) across the yellow arrow indicated in the micrographs. To see this figure in color, go online.

In our experiments we only detected one event where the L_d marker is the one excluded from the membrane at the GUV-GUV interface, i.e., only 6% of the observed hemifusion events (Fig. 5 and Video S4). The exclusion of the L_d marker starts at one edge of the region where the two GUVs are in contact and it gradually advances toward the other edge. In this event, the hemifusion diaphragm does not become flattened but the L_o GUV pushes and bends the L_d GUV. In addition, the fusion process is not completed but the GUVs remain adhered by the hemifusion diaphragm (note that, as the fusion is incomplete, this movie was not counted within the 32 fusion events mentioned earlier in the text). The deformation of the L_d GUV by the L_o GUV might indicate that the former vesicle is not tense enough for the fusion pore to open and expand. We also observe a lipid transfer from the L_d to the L_o GUV, which leads to the formation of an apparent asymmetric domain in the L_o GUV, similar to what we observed in the other hemifusion events, where the Npy relative fluorescence decreases to nearly 50% and the Rh fluorescence increases, reaching about 50% of its value in the L_d GUV (Fig.5). The asymmetric domain (ROI c in Fig. 5) is transient and we do not see interleaflet coupling, but the Rh-DOPE-labeled membrane retreats to its original GUV and the membrane recovers its L_o symmetric appearance. Eventually, the phase boundaries locate at the edges of the hemifusion diaphragm and the membranes seem to reach an equilibrium state.

To our knowledge, this is the first time that asymmetric domain formation and interleaflet coupling have been imaged in real time in GUVs and during fusion processes. Enoki and Feigenson developed a method by which they

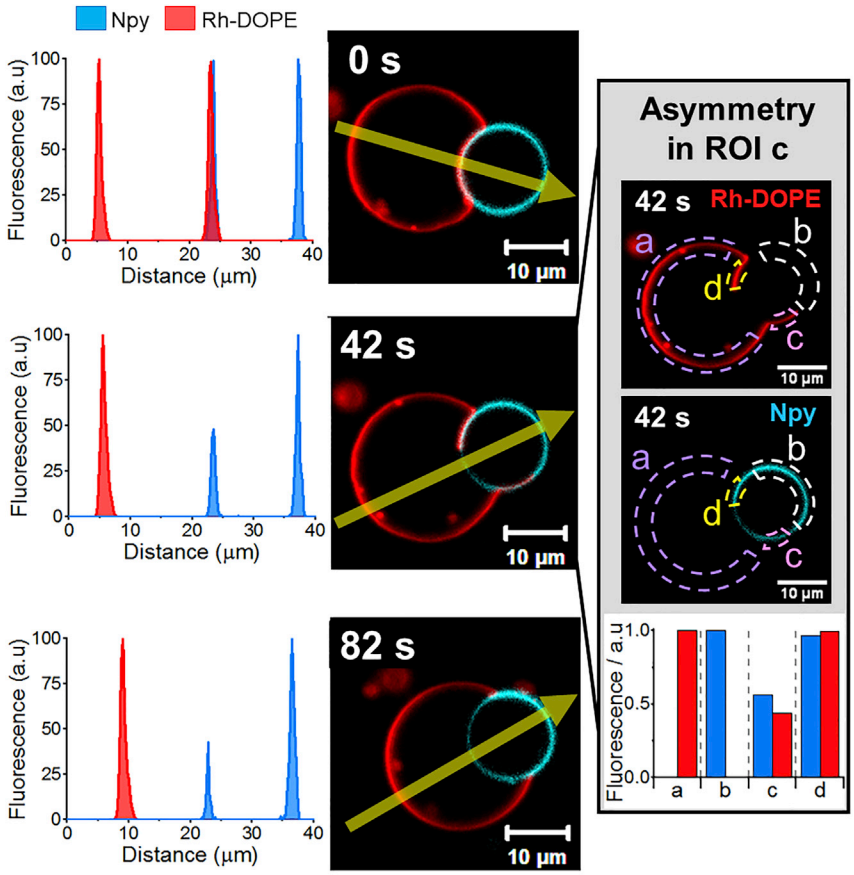

FIGURE 5 Confocal microscopy micrographs showing Rh-DOPE exclusion from the hemifusion diaphragm. The dye exclusion advances gradually from one edge to the other. The plots in the left show the fluorescence intensity profile of Npy and Rh-DOPE across the yellow arrow indicated in the micrographs. Inset shows micrographs of the separated imaging channels at 42 s (Rh-DOPE on the top and Npy in the middle) and a detailed analysis of the fluorescence intensity (bottom bar plot) of each imaging channel in different regions of the membrane as shown in the micrographs. The fluorescence intensity in ROI c shows a membrane domain where the relative intensity of each dye is approximately 50% of their maximum fluorescence intensity (ROI b = Npy-max; ROI c = Rhmax) that likely indicates membrane asymmetry. To see this figure in color, go online.

created asymmetric GUVs via hemifusion of the vesicles with a supported lipid bilayer (SLB) (16). Using this method, they saw that, after hemifusion, the phase-separated inner monolayer of the GUVs induces phase separation in an otherwise L_d outer monolayer; however, they only showed the final membrane configuration but the process leading to the interleaflet coupling is not revealed (16,17). In their system, the L_o domains modulate the lipid order in the opposing leaflet whereas our results show the opposite tendency. Nevertheless, they also see that the L_o domains in the asymmetric membrane are less ordered than the symmetric L_o phase. Previous studies on asymmetric lipid membranes show disparity regarding which phase dominates the final bilayer phase. For instance, L_o domains in the outer leaflet of SLBs have been seen to induce phase separation in the inner leaflet (29,30). However, the substrate where SLBs are formed can have a significant influence on the dynamical behavior of the lipids in the inner leaflet. Chiantia and London showed that long-chain sphingomyelin (SM) in the outer leaflet of vesicles decreases the lateral diffusion of DOPC lipids in the inner monolayer (31). They also saw that the interleaflet coupling is stronger when the PC lipids in the inner monolayer have one saturated acyl chain and attributed the coupling effect to the interaction between acyl chains at the bilayer midplane (31).

On the contrary, a disorganization effect of ordered domains by disordered lipids in the opposite leaflet, analogous to what we observe in most of our results, was reported by Heberle in asymmetric LUVs where the outer leaflet was composed of DPPC and the inner leaflet of POPC (32). Using small-angle neutron scattering, they observed that the L_d inner monolayer induced a significant decrease in the lipid packing density of the gel domains in the outer leaflet (32). Similarly, St Clair et al. have shown that, while symmetric LUVs formed by a mixture of SM, POPC, and cholesterol are phase separated, in asymmetric LUVs with SM:POPC:Chol in the outer leaflet but a POPC:Chol inner monolayer the formation of L_o domains is completely suppressed (33). Wang and London also reported the ability of DOPC:Chol L_d inner leaflet of asymmetric LUVs to destabilize and destroy ordered domains in the outer monolayer containing SM (34). This disorganization of the outer leaflet L_o domains is, however, less pronounced when its content in SM increases (34). Collins and Keller studied asymmetric pore spanning planar membranes formed by a L_d inner leaflet and an outer leaflet with a lipid composition within the L_d - L_o coexistence region of the phase diagram and showed that increasing or decreasing the fraction of high-T_m lipid in the outer monolayer induces or suppresses, respectively, the formation of bilayer domains (35).

Our observations (and the studies mentioned above) confirm that, in bilayers of asymmetric composition, the phase of one leaflet can alter the phase state of the opposite leaflet to create phase symmetry in a bilayer domain. Nevertheless, the mechanisms that dictate which leaflet and which phase dominates over the other remain elusive. The type of model membrane employed, as well as the varying lipid composition and experimental conditions used in different interleaflet coupling studies, likely gives rise to apparently contradictory differences in phenomena that have been reported so far. While studies on SLBs have shown the L_o domain dominating the phase state of asymmetric membranes (30,36,37), asymmetric unsupported membranes, such as vesicles, show more variability where the L_d phase more commonly dominates but both L_d and L_o phase monolayers can dictate the bilayer properties. This suggests that the rigidity of solid supports favors the more rigid L_o phase dominating the properties of asymmetric membranes. This is consistent with previous reports of more ordered phases being favored in symmetric bilayer membranes within regions of local adhesion, where the free energy for formation of ordered membrane domains is lowered by mechanical suppression of thermal membrane undulations (38). Furthermore, in our current work, the only observation of the L_o phase dominating behavior is seen where the L_o phase GUV is under tension such that it does not visibly deform from its sphericity during hemifusion, giving rise to an interface with greater mechanical rigidity. Unsupported membranes may be more physiologically relevant to the behavior of biomembranes within a cellular context; however, mechanoresponsive mechanisms are known to play important roles in biological signaling processes. The ability of asymmetric membranes to change phase state in response to local changes in mechanical cues in their environment, such as during cell adhesion, the invasion of pathogens, or cytoskeletal interactions with the membrane could play a fundamental role in rapid cell signaling responses.

CONCLUSION

Here, we have demonstrated that 30 nm SiO_2 NPs mediate fusion between L_d DOPC GUVs and L_o DPPC:Chol (7:3) GUVs and generate phase-separated GUVs. Furthermore, we have shown that imaging of L_d GUVs and L_o GUVs undergoing hemifusion, allows real-time visualization of asymmetric domain formation and interleaflet coupling. While membrane mechanical properties, such as bending rigidity, lateral tension, and curvature, has been proposed to play a central part during membrane fusion (18,39–41), less attention has been paid to the role of the different lipid composition and biophysical properties of each membrane undergoing fusion. We find that transmembrane stresses generated in asymmetric membrane intermediates enhance the efficiency of full fusion between vesicles compared with symmetric membrane fusion in our previous studies (18). In addition, we find that the L_d phase dominates the properties of bilayers with phase asymmetry; by comparison with broader findings in the literature, this may imply that the mechanical properties of the local environment could be an important parameter in determining the phase that dominates the local bilayer properties.

Further investigations following this experimental approach using a wider range of vesicle compositions would provide additional valuable insight into the role of each leaflet's composition, phase state, and mechanical properties on interleaflet coupling in the mechanisms governing the lipid lateral organization and phase states within biological membranes. For example, recent theoretical work implicates cholesterol as an important coupling agent between membrane leaflets that can rapidly redistribute in response to a combination of the monolayer membrane composition and mechanical stresses (28). Therefore investigating a range of initial cholesterol compositions in the two initial GUVs could elucidate phenomena in asymmetric membranes driven by the transbilayer redistribution of cholesterol. A range of different starting GUV compositions would also provide a range of compositional pathways through the phase diagram that lie on a straight line between the compositions of the two fusing GUVs. These could be designed to encompass the three-phase L_d-L_o-$L_{\beta'}$ region of the phase diagram or to approach the critical point of the L_d - L_o phase boundary, elucidating the role of these features in the underlying phase diagram in the phenomenology of asymmetric membranes and membrane fusion.

DATA AVAILABILITY

Data is available from the authors on reasonable request.

SUPPORTING MATERIAL

Supporting material can be found online at https://doi.org/10.1016/j.bpj.2022.10.006.

AUTHOR CONTRIBUTIONS

M.A.P. performed the experiments and the data analysis. M.A.P. and P.A.B. contributed to designing the experiments, discussion and writing the manuscript. P.A.B. supervised the research.

ACKNOWLEDGMENTS

M.A.P. acknowledges the University of Leeds for funding through the Lowson Scholarship. The Zeiss LSM 880 with Airyscan inverted confocal microscope was funded by the Wellcome Trust (WT104818MA).

DECLARATION OF INTERESTS

The authors declare no competing interests.

REFERENCES

1. Sych, T., C. O. Gurdap, …, E. Sezgin. 2021. How does liquid-liquid phase separation in model membranes reflect cell membrane heterogeneity? *Membranes.* 11:323. https://doi.org/10.3390/membranes11050323.
2. Baumgart, T., S. T. Hess, and W. W. Webb. 2003. Imaging coexisting fluid domains in biomembrane models coupling curvature and line tension. *Nature.* 425:821–824. https://doi.org/10.1038/nature02013.
3. Sezgin, E., I. Levental, …, C. Eggeling. 2017. The mystery of membrane organization: composition, regulation and roles of lipid rafts. *Nat. Rev. Mol. Cell Biol.* 18:361–374. https://doi.org/10.1038/nrm.2017.16.
4. Nickels, J. D., J. C. Smith, and X. Cheng. 2015. Lateral organization, bilayer asymmetry, and inter-leaflet coupling of biological membranes. *Chem. Phys. Lipids.* 192:87–99. https://doi.org/10.1016/j.chemphyslip.2015.07.012.
5. Cebecauer, M., M. Amaro, …, M. Hof. 2018. Membrane lipid nanodomains. *Chem. Rev.* 118:11259–11297. https://doi.org/10.1021/acs.chemrev.8b00322.
6. Sarmento, M. J., M. Hof, and R. Šachl. 2020. Interleaflet coupling of lipid nanodomains - insights from in vitro systems. *Front. Cell Dev. Biol.* 8:284. https://doi.org/10.3389/fcell.2020.00284.
7. Doktorova, M., J. L. Symons, and I. Levental. 2020. Structural and functional consequences of reversible lipid asymmetry in living membranes. *Nat. Chem. Biol.* 16:1321–1330. https://doi.org/10.1038/s41589-020-00688-0.
8. Fadeel, B., and D. Xue. 2009. The ins and outs of phospholipid asymmetry in the plasma membrane: roles in health and disease. *Crit. Rev. Biochem. Mol. Biol.* 44:264–277. https://doi.org/10.1080/10409230903193307.
9. Verkleij, A. J., R. F. Zwaal, …, L. L. van Deenen. 1973. The asymmetric distribution of phospholipids in the human red cell membrane. A combined study using phospholipases and freeze-etch electron microscopy. *Biochim. Biophys. Acta.* 323:178–193. https://doi.org/10.1016/0005-2736(73)90143-0.
10. Devaux, P. F. 1991. Static and dynamic lipid asymmetry in cell memebranes. *Biochemistry.* 30:1163–1173. https://doi.org/10.1021/bi00219a001.
11. Lorent, J. H., K. R. Levental, …, I. Levental. 2020. Plasma membranes are asymmetric in lipid unsaturation, packing and protein shape. *Nat. Chem. Biol.* 16:644–652. https://doi.org/10.1038/s41589-020-0529-6.
12. Devaux, P. F., and R. Morris. 2004. Transmembrane asymmetry and lateral domains in biological membranes. *Traffic.* 5:241–246. https://doi.org/10.1111/j.1600-0854.2004.0170.x.
13. Clair, S., J.R., …, E. London. 2017. Preparation and physical properties of asymmetric model membrane vesicles. *In* The Biophysics of Cell Membranes: Biological Consequences. R. M. Epand and J.-M. Ruysschaert, eds Springer Singapore, Singapore, pp. 1–27.
14. Bezlyepkina, N., R. S. Gracià, …, R. Dimova. 2013. Phase diagram and tie-line determination for the ternary mixture DOPC/eSM/Cholesterol. *Biophys. J.* 104:1456–1464. https://doi.org/10.1016/j.bpj.2013.02.024.
15. Dreher, Y., K. Jahnke, …, K. Göpfrich. 2021. Division and regrowth of phase-separated giant unilamellar vesicles**. *Angew. Chem., Int. Ed. Engl.* 60:10661–10669. https://doi.org/10.1002/anie.202014174.
16. Enoki, T. A., and G. W. Feigenson. 2019. Asymmetric bilayers by hemifusion: method and leaflet behaviors. *Biophys. J.* 117:1037–1050. https://doi.org/10.1016/j.bpj.2019.07.054.
17. Enoki, T. A., J. Wu, …, G. W. Feigenson. 2021. Investigation of the domain line tension in asymmetric vesicles prepared via hemifusion. *Biochim. Biophys. Acta Biomembr.* 1863:183586. https://doi.org/10.1016/j.bbamem.2021.183586.
18. Arribas Perez, M., and P. A. Beales. 2021. Biomimetic curvature and tension-driven membrane fusion induced by silica nanoparticles. *Langmuir.* 37:13917–13931. https://doi.org/10.1021/acs.langmuir.1c02492.
19. Angelova, M. I., and D. S. Dimitrov. 1986. Liposome electroformation. *Faraday Discuss. Chem. Soc.* 81:303–311. https://doi.org/10.1039/dc9868100303.
20. Sezgin, E., D. Waithe, …, C. Eggeling. 2015. Spectral imaging to measure heterogeneity in membrane lipid packing. *ChemPhysChem.* 16:1387–1394. https://doi.org/10.1002/cphc.201402794.
21. Baumgart, T., G. Hunt, …, G. W. Feigenson. 2007. Fluorescence probe partitioning between lo/ld phases in lipid membranes. *Biochim. Biophys. Acta.* 1768:2182–2194. https://doi.org/10.1016/j.bbamem.2007.05.012.
22. Veatch, S. L., and S. L. Keller. 2003. Separation of liquid phases in giant vesicles of ternary mixtures of phospholipids and cholesterol. *Biophys. J.* 85:3074–3083. https://doi.org/10.1016/s0006-3495(03)74726-2.
23. Uppamoochikkal, P., S. Tristram-Nagle, and J. F. Nagle. 2010. Orientation of tie-lines in the phase diagram of DOPC/DPPC/cholesterol model biomembranes. *Langmuir.* 26:17363–17368. https://doi.org/10.1021/la103024f.
24. Veatch, S. L., O. Soubias, …, K. Gawrisch. 2007. Critical fluctuations in domain-forming lipid mixtures. *Proc. Natl. Acad. Sci. USA.* 104:17650–17655. https://doi.org/10.1073/pnas.0703513104.
25. Elani, Y., S. Purushothaman, …, O. Ces. 2015. Measurements of the effect of membrane asymmetry on the mechanical properties of lipid bilayers. *Chem. Commun.* 51:6976–6979. https://doi.org/10.1039/c5cc00712g.
26. Hossein, A., and M. Deserno. 2020. Spontaneous curvature, differential stress, and bending modulus of asymmetric lipid membranes. *Biophys. J.* 118:624–642. https://doi.org/10.1016/j.bpj.2019.11.3398.
27. Silvius, J. R. 2003. Role of cholesterol in lipid raft formation: lessons from lipid model systems. *Biochim. Biophys. Acta.* 1610:174–183. https://doi.org/10.1016/S0005-2736(03)00016-6.
28. Varma, M., and M. Deserno. 2022. Distribution of cholesterol in asymmetric membranes driven by composition and differential stress. *Biophys. J.* 121:4001–4018. https://doi.org/10.1016/j.bpj.2022.07.032.
29. Kiessling, V., J. M. Crane, and L. K. Tamm. 2006. Transbilayer effects of raft-like lipid domains in asymmetric planar bilayers measured by single molecule tracking. *Biophys. J.* 91:3313–3326. https://doi.org/10.1529/biophysj.106.091421.
30. Wan, C., V. Kiessling, and L. K. Tamm. 2008. Coupling of cholesterol-rich lipid phases in asymmetric bilayers. *Biochemistry.* 47:2190–2198. https://doi.org/10.1021/bi7021552.
31. Chiantia, S., and E. London. 2012. Acyl chain length and saturation modulate interleaflet coupling in asymmetric bilayers: effects on dynamics and structural order. *Biophys. J.* 103:2311–2319. https://doi.org/10.1016/j.bpj.2012.10.033.
32. Heberle, F. A., D. Marquardt, …, G. Pabst. 2016. Subnanometer structure of an asymmetric model membrane: interleaflet coupling influences domain properties. *Langmuir.* 32:5195–5200. https://doi.org/10.1021/acs.langmuir.5b04562.
33. St Clair, J. W., S. Kakuda, and E. London. 2020. Induction of ordered lipid raft domain formation by loss of lipid asymmetry. *Biophys. J.* 119:483–492. https://doi.org/10.1016/j.bpj.2020.06.030.
34. Wang, Q., and E. London. 2018. Lipid structure and composition control consequences of interleaflet coupling in asymmetric vesicles. *Biophys. J.* 115:664–678. https://doi.org/10.1016/j.bpj.2018.07.011.
35. Collins, M. D., and S. L. Keller. 2008. Tuning lipid mixtures to induce or suppress domain formation across leaflets of unsupported asymmetric bilayers. *Proc. Natl. Acad. Sci. USA.* 105:124–128. https://doi.org/10.1073/pnas.0702970105.
36. Kiessling, V., C. Wan, and L. K. Tamm. 2009. Domain coupling in asymmetric lipid bilayers. *Biochim. Biophys. Acta.* 1788:64–71. https://doi.org/10.1016/j.bbamem.2008.09.003.
37. Vázquez, R. F., E. Ovalle-García, …, S. M. Maté. 2021. Asymmetric bilayers mimicking membrane rafts prepared by lipid exchange: nanoscale characterization using AFM-Force spectroscopy. *Biochim. Biophys. Acta Biomembr.* 1863:183467. https://doi.org/10.1016/j.bbamem.2020.183467.

38. Gordon, V. D., M. Deserno, …, W. C. K. Poon. 2008. Adhesion promotes phase separation in mixed-lipid membranes. *Europhys. Lett.* 84:48003. https://doi.org/10.1209/0295-5075/84/48003.

39. Kliesch, T. T., J. Dietz, …, A. Janshoff. 2017. Membrane tension increases fusion efficiency of model membranes in the presence of SNAREs. *Sci. Rep.* 7:12070. https://doi.org/10.1038/s41598-017-12348-w.

40. Kozlov, M. M., and L. V. Chernomordik. 2015. Membrane tension and membrane fusion. *Curr. Opin. Struct. Biol.* 33:61–67. https://doi.org/10.1016/j.sbi.2015.07.010.

41. Chernomordik, L. V., and M. M. Kozlov. 2008. Mechanics of membrane fusion. *Nat. Struct. Mol. Biol.* 15:675–683. https://doi.org/10.1038/nsmb.1455.